

# A Microfabricated Wireless RF Pressure Sensor Made Completely of Biodegradable Materials

Mengdi Luo, Adam W. Martinez, Chao Song, Florian Herrault, *Member, IEEE*,  
and Mark G. Allen, *Fellow, IEEE*

**Abstract**—A wireless RF MEMS pressure sensor made entirely of biodegradable materials is presented. Such biodegradable sensors may be appropriate for short-term, acute medical implantation applications as they potentially eliminate the need for implant extraction when sensing is no longer required. The biodegradable sensors described here require structural materials for pressure sensing, dielectric materials for insulation, and conducting materials for formation of electrical elements and wireless links. Zinc/iron bilayers were used as the sensor conductor material, and known biodegradable polymers poly-L-lactide and polycaprolactone were used as dielectric and structural materials. Zinc, which otherwise degrades very slowly on its own under biological conditions, is galvanically activated when electrically connected to iron in saline, greatly increasing the total degradation rate of the conductors. To avoid contact of the biodegradable materials with the strong chemicals or solvents that are typically used in conventional MEMS fabrication, embossing, multilayer folding, and lamination were combined with traditional techniques during fabrication. The fabricated sensor was wirelessly tested in both air and 0.9% saline and demonstrated a linear frequency response with external applied pressure. A sensitivity of 39 kHz/kPa was measured in the 0–20 kPa pressure range in air and initially in saline. After immersion in saline for 20 h, the sensor stabilized, remaining stable and functional for 86 h with a sensitivity of  $-54 \pm 4$  kHz/kPa. [2013-0128]

**Index Terms**—Biodegradable sensor, galvanic corrosion, microfabrication, wireless RF pressure sensor.

## I. INTRODUCTION

**I**MPLANTABLE resonant passive sensors were proposed more than five decades ago as a solution to wirelessly measure physical parameters within living organisms [1]. Since then, non-degradable MEMS-fabricated passive resonant sensors have been demonstrated for chronic implantable applications to monitor blood pressure and other physiological conditions [2, 3]. However, in some acute or shorter-term medical applications (e.g., wound or bone healing) where sensor functionality is required only for a limited time, the implantation of biodegradable sensors could be preferable, as

such sensors could remove the need for a secondary surgery for sensor removal.

Biodegradable electronics that combine biodegradable polymers as package and biodegradable metals as conductors is a very promising approach to such biodegradable sensors. Biodegradable materials for medical application include compounds that are both biocompatible and that can degrade into products that can be eliminated from body by either natural pathways or involved normally in a metabolic pathway [4]. The family of aliphatic polyesters that chemically degrade by hydrolytic cleavage of backbone ester bonds [5, 6] and enzymatic promotion [7] has been the dominant choice for biodegradable polymers in medical applications. Examples of such materials include polylactic acid (PLA), existing in three stereochemical forms semi-crystalline poly(L-lactide) PLLA, poly (D-lactide) (PDLA) and amorphous poly(DL-lactide) (PDLA); Polyglycolide, (PGA); polycaprolactone (PCL); poly(3-hydroxybutyrate) (PHB); and co-polymers and blends of these materials [4, 8, 9]. The degradation time of these materials can range from less than 3 months to more than 24 months [8]. In addition to polymers, the term biodegradable can also apply to metals and metallic alloys that exhibit similar behavior. Magnesium (Mg) and iron (Fe) are the most well-known biocompatible and biodegradable metals; for example, Fe, Fe alloys, and Mg alloys have been demonstrated in biodegradable stent applications [10–12].

There have been several efforts to realize the goal of fully biodegradable implants for a variety of applications. Implantable biodegradable stimulators that exploit RF coupling have been proposed as an approach to promote bone growth. The coupling coil was fabricated using conventional micromilling of biodegradable magnesium alloys, and packaged with PLDA [13]. Miniaturized resistor–inductor–capacitor (RLC) resonators with sizes of approximately 10–17 mm were fabricated using biodegradable materials and proposed as an RF component of wireless biosensors; the degradable materials include the metals Mg, Fe, Mg- and Fe-alloys, and polymer composites PLLA-PPy (polypyrrole) and PCL-PPy [14]. Water soluble electronics using thin layers of physical vapor deposited Mg, magnesium oxide (MgO), and silicon dioxide (SiO<sub>2</sub>) as conductors and dielectrics, and transfer printed monocrystalline silicon nanomembranes (Si NMs) as semiconductors were fabricated on water soluble silk. Example platforms including transistors, diodes, inductors, capacitors, resistors and interconnects [15].

In this work, a functional pressure sensor based on the passive resonant mechanism [16] using completely biodegradable

Manuscript received July 8, 2013; revised September 16, 2013; accepted October 11, 2013. Date of publication November 25, 2013; date of current version January 30, 2014. Subject Editor D.-I. Cho.

M. Luo is with the School of Materials Science and Engineering, Georgia Institute of Technology, Atlanta, GA 30332 USA (e-mail: mandyluo@gatech.edu).

A. Martinez, C. Song, F. Herrault, and M. G. Allen are with the School of Electrical and Computer Engineering, Georgia Institute of Technology, Atlanta, GA 30332 USA (e-mail: adamw@gatech.edu; csong7@gatech.edu; florian@gatech.edu; mark.allen@ece.gatech.edu).

Color versions of one or more of the figures in this paper are available online at <http://ieeexplore.ieee.org>.

Digital Object Identifier 10.1109/JMEMS.2013.2290111

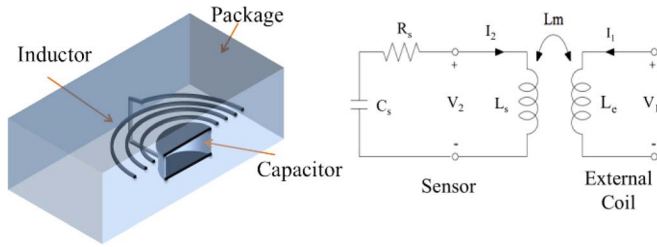


Fig. 1. Schematic cross section diagram (left) and equivalent circuit (right) of a passive LC resonant sensor.

materials is microfabricated. It utilizes RF interrogation while simultaneously maintaining its all-biodegradable character. The pressure sensor consists of a sensing cavity, bounded by two electrodes forming a variable capacitor and connected to an inductor coil (Fig. 1). The inductor coil not only acts as an essential component of the resonant sensor, but also provides means for magnetically coupling the sensor to an external (e.g., outside the body) coil. When pressure is applied to the sensor, the gap between the two capacitive electrodes is reduced and the capacitor value increases. The resulting pressure-induced change in the LC resonant frequency can be measured wirelessly using the external coil.

To create this device, biodegradable structural materials, conductors, and dielectrics are required to form and interconnect electrical elements, sensing elements, and an embedding package. PLLA is used as the packaging and pressure-sensing plate material because of its good mechanical properties [9], and PCL is utilized as a bonding and sealing material because of its low melting temperature (approximately 61 °C), which is compatible with the proposed fabrication process. For wireless sensing, high electrical element quality factor ( $Q$ ) at higher frequency (e.g., tens of MHz and above) is required. Although it is biodegradable, pure Fe is a poor choice for electrical conductors at high frequency due to the enhancement of the skin effect (and concomitant increase in AC resistance) due to its large magnetic permeability [17]. Zinc (Zn) has reasonable electrical characteristics for high- $Q$  elements, and is also considered a biocompatible metal and an essential element consumed by the human body [18].

Previous work on Zn-containing implants showed that addition of small quantities of Zn to Mg-based alloys slowed degradation [19, 20]. More recently, implants containing substantial amounts of Zn have been studied. Zberg *et al.* investigated bulk metallic glasses containing up to 35% Zn [21] and demonstrated biocompatibility and reduced hydrogen formation compared to Mg [21, 22]. Bowen *et al.* fabricated metallic Zn stents and deployed them in the rat aorta. After six months, these Zn stents demonstrated longevity that was comparable to Fe, and a benign bio response that was comparable to Mg [23].

However, the degradation rate of pure Zn in biologically-relevant environments is slow [24]. To overcome these limitations, Fe-based galvanic corrosion of Zn in saline environments was exploited. A relatively small amount of Fe and a relatively large amount of Zn were combined to form an electrical bi-layer. During sensor operation, the Zn layer acts as a low-resistance path enabling the formation of

TABLE I  
DIMENSIONS OF THE CONDUCTORS OF THE PRESSURE SENSOR

Zn/Fe Bilayer Inductor			Zn/Fe Bilayer Capacitor		
Number of turns	Line Width ( $\mu\text{m}$ )	Spacing Width ( $\mu\text{m}$ )	Gap Distance ( $\mu\text{m}$ )	Pad Radius (mm)	Pad Thickness ( $\mu\text{m}$ )
14	70	80	30	2.5	65

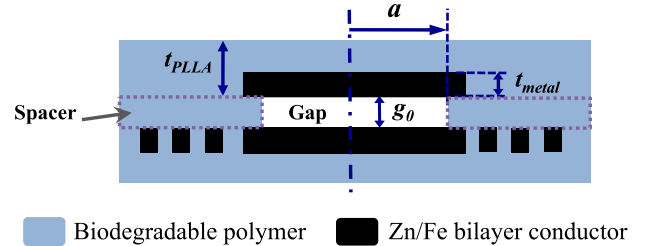


Fig. 2. Pressure sensor schematic cross section for design.

high- $Q$  elements. During degradation, the Fe stimulates Zn corrosion (i.e, the Zn works as a sacrificial anode), resulting in rapid and controllable corrosion [25]. In addition to these desirable electrical and corrosion properties, both Fe and Zn can be easily electrodeposited from aqueous solution [26, 27], providing a path to the relatively thick, MEMS-fabricated micro-scale conductors required for high- $Q$  elements.

## II. DESIGN AND FABRICATION

### A. Materials

PLLA with molecular weight of approximately 690,000 g/mol and PCL with average molecular weight of approximately 176,600 g/mol were purchased from PURAC and LACTEL, respectively. The polymers were dissolved in dichloromethane (DCM, Aldrich) with different concentration and solvent cast to form PLLA and PCL films with different thickness. Zn and Fe were electrodeposited from standard plating baths [26, 27].

### B. Conductor Design

The operating frequency of passive wireless devices is typically bounded by maximum device size (at low frequencies) and signal degradation in the lossy medium of the body (at high frequencies). It has been demonstrated that operating frequencies in the 10-100 MHz range are suitable for *in-vivo* wireless measurements [2, 3]. To achieve such resonant frequencies while maintaining the device area below a nominal value of 1 cm<sup>2</sup>, both the inductor and capacitor must follow specific design guidelines. Table I shows a feasible set of design parameters for the conductors of the RF pressure sensor that meet these constraints.

### C. Finite Element Simulation of Capacitance Change

A schematic cross-section of the pressure sensor is shown in Fig. 2. The device consists of a bottom PLLA layer with an electroplated Zn/Fe bilayer inductor and capacitor

TABLE II  
DIMENSIONS OF THE SENSOR DESIGNS FOR SIMULATION

Design #	Cavity Radius ( $a$ ) (mm)	Thickness of PLLA ( $t_{PLLA}$ ) ( $\mu\text{m}$ )
1	2.1	200
2	2.1	400
3	1.8	200

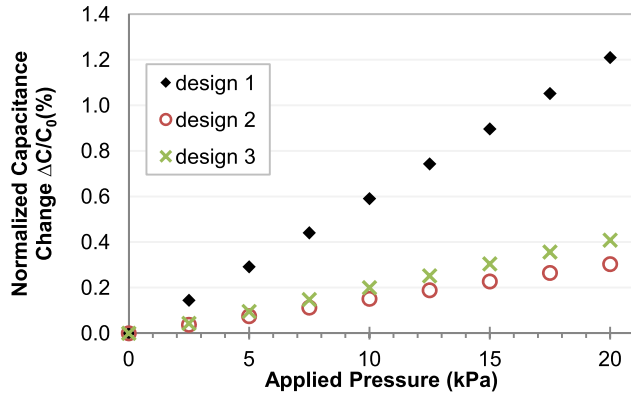


Fig. 3. Normalized capacitance change as a function of external applied pressure for the simplified sensor structure of Fig. 2 for different cavity dimensions and PLLA thicknesses. The various designs are given in Table II.

plate, a PLLA/PCL spacer layer that forms the sensor cavity, and a top PLLA layer with a top Zn/Fe bilayer capacitor plate. The Zn/Fe electrical interconnects between the inductor and the capacitor plates are not depicted. A first-order analytical model indicates that the center deflection of the plates varies linearly with pressure when the deflection of the plates is small compared with their thicknesses. The deflection is inversely proportional to the flexural rigidity, which is related to the Young's modulus  $E$  and the Poisson's ratio  $\nu$  of the material. Finite element simulations (COMSOL 4.2), coupling electrical with mechanical analyses, were performed to determine the capacitance change (and ultimately the frequency change) of the sensor as a function of applied pressure. A two-dimensional axisymmetric model was used. The geometry of the simulation was simplified by neglecting the Zn/Fe inductor coil and via structures. The Young's modulus difference between Zn and Fe is also neglected. The  $E$  and  $\nu$  of PLLA as well as of the Zn/Fe bilayer (referred to as 'metal' in the simulation) were assumed to be 3 GPa, 0.35 [28], and 100 GPa, 0.25 [29], respectively, based on literature values. The dielectric constant of PLLA was assumed to be 3.0 [30]. Two different radii of deflecting diaphragm ( $a$ ) and two different diaphragm thicknesses ( $t_{PLLA}$ ), chosen with fabrication constraints as well as desired performance in mind, were selected for detailed modeling (Table II). The initial gap between capacitor plates was set at 30  $\mu\text{m}$ .

The simulated capacitance change of the simplified sensor structure is presented in Fig. 3. Applied pressures ranging from 0 to 20 kPa were simulated, corresponding to typical physiological pressure ranges found in the body [31, 32]. The radius of the cavity, which ultimately defines the radius

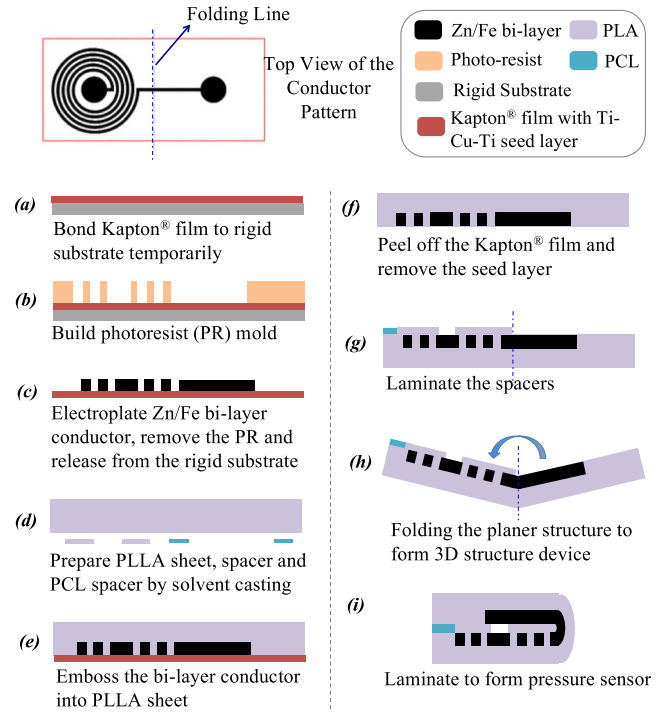


Fig. 4. Fabrication process of the passive pressure sensor completely made of biodegradable materials.

of the deflecting diaphragm, is set smaller than the radius of the capacitor plate. The thinner PLLA sheet (Design 1) exhibits a higher capacitance change than the thicker PLLA sheet (Design 2) for the same cavity radius because of larger deflection. The smaller the radius of the cavity (Design 3) shows lower capacitance change than the larger cavity radius (Design 1) with the same PLLA thickness. The capacitance shows linear change as a function of applied pressure, due to the relatively small deflection of the plates compared to their thickness, as well as the gap.

#### D. Pressure Sensor Fabrication

The process for sensor fabrication is schematically depicted in Fig. 4. Nontraditional fabrication approaches have been developed to augment conventional approaches, since some biodegradable materials may be sensitive to chemicals, temperatures, or environments typically utilized in standard micro-fabrication. The process relies on iron and zinc electroplating followed by polymer embossing. A folding technique coupled with polymer multilayer lamination was utilized to create the sensor cavity and the appropriate LC resonant circuit.

The process began with the through-photoresist electrodeposition of zinc/iron bilayer conductor patterns (inductor coils and capacitor plates). An 80- $\mu\text{m}$ -thick flexible and chemically-resistant polymer film (Kapton<sup>®</sup>) with a titanium/copper/titanium (Ti/Cu/Ti) seed layer was temporarily bonded onto a rigid substrate (wafer) using a thin layer of photoresist as an adhesive layer (Fig. 4(a)). A photoresist mold with thickness of approximately 90  $\mu\text{m}$  was formed on the Kapton<sup>®</sup> film using photolithography (Fig. 4(b)). After removal of the topmost layer of Ti at the bottom of the mold

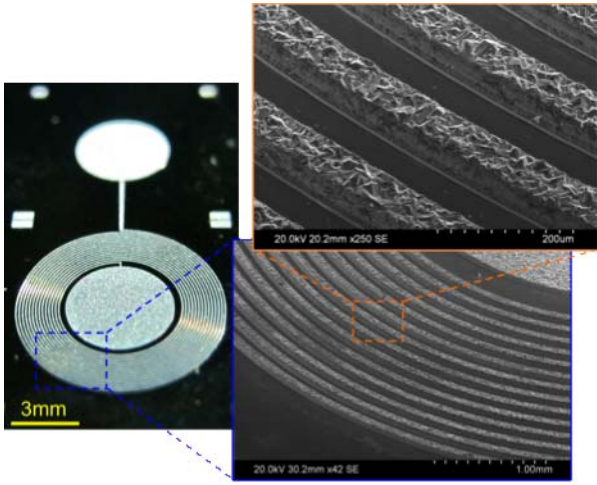


Fig. 5. Electroplated Zn/Fe inductor on metalized Kapton® film. The insets show two scanning electron microscope images of the electrodeposited Zn/Fe windings at a 30 degree tilt.

using diluted hydrogen fluoride (HF, 1:50) solution, 5-10  $\mu\text{m}$  of Fe was electroplated into the mold at a current density of  $5\text{mA}/\text{cm}^2$ , followed by electroplating of approximately  $50\ \mu\text{m}$  Zn on top of the iron via pulse reverse electroplating at an average current density of  $6\text{mA}/\text{cm}^2$ . Upon completion of electroplating, the photoresist was removed in acetone and the Kapton® film bearing the microfabricated Zn/Fe bilayer conductor patterns was separated from the rigid substrate (Fig. 4(c)). Fig. 5 shows images of the electroplated Zn/Fe bilayer inductor on metalized Kapton® film with a close tilted view of the bilayer windings. The two metal layers can be clearly seen in the upper right scanning electron microscopy (SEM) image: a thinner, bottommost Fe layer and a thicker Zn layer with a larger grain size on top.

The polymeric portions of the sensor comprise three polymer films, fabricated using solvent casting from dichloromethane (DCM) to desired thicknesses, and patterned as appropriate using a  $\text{CO}_2$  laser (Fig. 4(d)). The first film (embossing film) is made of PLLA to a thickness of 200-300  $\mu\text{m}$ , is not patterned, and will be used to support the entire sensor conductor assembly fabricated above. The second film (PLLA spacer) is also fabricated from PLLA to a thickness of 30  $\mu\text{m}$  and patterned into a toroidal ring to define the cavity. The third film (PCL spacer) is fabricated from PCL to a thickness of 40  $\mu\text{m}$  and is patterned to almost completely concentrically surround the outside of the PLLA spacer. Photomicrographs of the fabricated polymer sheets are shown in Fig. 6.

The Kapton® film with electroplated Zn/Fe bilayer conductors and the embossing film fabricated as above were laminated under 10-bar pressure at 180  $^\circ\text{C}$  for 5 minutes. After lamination, and the resultant embossing of the metal bilayer into the embossing film, the Kapton® film substrate was peeled off. Any remaining nonbiodegradable seed layer originally between the Kapton® and the electroplated material was removed by micro-polishing, thereby limiting the number of wet processing steps (Fig. 4(f)). The resulting structure

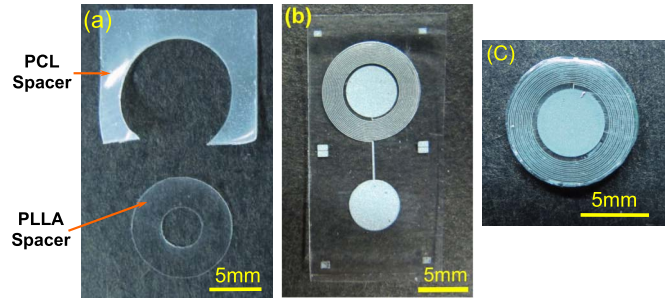


Fig. 6. (a) Spacers made of biodegradable polymers PLLA and PCL, (b) embossing PLLA film bearing the Zn/Fe bilayer pattern, (c) microfabricated RF pressure sensor after folding, lamination, and laser trimming.

consisted of the microfabricated Zn/Fe bilayer conductor patterns embedded in the embossing film, as shown in Fig. 6(b).

The embossing film bearing the Zn/Fe bilayer was then prepared for assembly and lamination. The film was spray-coated with a thin layer (less than 1  $\mu\text{m}$ ) of PCL in DCM in the regions external to the capacitor plates. The ring-shaped PLLA spacer and the PCL spacer were then solvent bonded to the embossing film by means of a very small quantity of DCM ( $\sim 50\ \mu\text{L}$ ) (Fig. 4(g)). Using this small amount of solvent limited solvation to the surface, preventing change to the geometry of the spacer, cavity, and device. Alternatively, solventless fabrication can also be considered for this step [33].

The embossing film bearing the embedded Zn/Fe bilayer and the bonded spacers was then folded (Fig. 4(h)) and laminated to form the PLLA-Zn/Fe pressure sensor. The lamination was performed under a nominal pressure of 10 bar at 55  $^\circ\text{C}$  for 1 minute. The folding was performed with the assistance of selective heating along the folding line. The folding technique, adapted from [34], enables the microfabrication of a 3-D device with multiple metal layers and electrical interconnects using a single electrodeposition step. This is particularly favorable when the metallic and polymeric materials are sensitive to chemicals used in conventional microfabrication techniques. During the lamination, the PCL spacer together with the thin PCL layer softened and sealed the cavity. Finally, the outer device shape was defined and further sealed by  $\text{CO}_2$  laser micromachining around the edge of the inductor. Fig. 6(a) depicts the 200- $\mu\text{m}$ -thick embossing film bearing the embedded Zn/Fe bilayer patterns along with the spacers before folding and lamination. An example of a fully-fabricated and functional 10-mm-diameter device is shown in Fig. 6(c). The design parameters are reported in Table I with cavity radius of 2.1 mm.

### III. CHARACTERIZATION

#### A. Degradation of Zn/Fe Bilayer Conductors

Although the degradation rates of the biodegradable polymers have been studied previously [4–8], there is less information available for biodegradable metals in biodegradable sensor applications. Freestanding Zn/Fe bilayer conductors are obtained by dissolving the PLLA of the fabricated structure of Fig. 6(b). The conductors were washed with DCM to remove

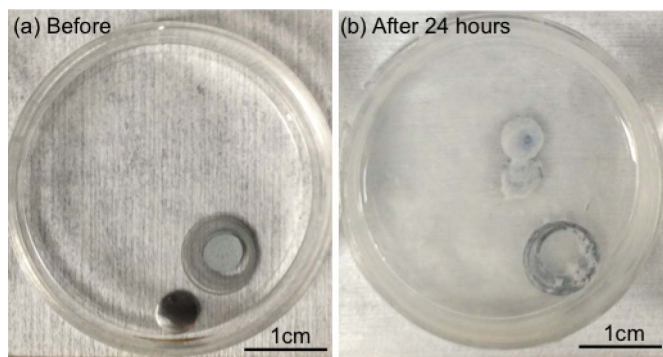


Fig. 7. Plated Zn/Fe bilayer freestanding conductors (a) before degradation, and (b) after degrading for 24 hours in 0.9% saline (without washing and drying).

PLLA residues and dried thoroughly before measurement. Freestanding electroplated Zn samples (no Fe) with size of  $0.3 \text{ cm} \times 2.5 \text{ cm}$  and thickness between  $70\text{--}100 \mu\text{m}$  were also fabricated as controls. The weight of each specimen was measured carefully before the degradation test. Each specimen was immersed in 10 mL of saline (0.9% NaCl, pH 6.8) and placed in an incubator at a temperature of  $37 \pm 0.5 \text{ }^\circ\text{C}$  with gentle mechanical agitation. The weight of each specimen was measured approximately every twelve hours over a 300-hour time frame. Each specimen was rinsed with approximately 50 mL deionized (DI) water for at least 3 times and dried thoroughly in a  $37 \pm 0.5 \text{ }^\circ\text{C}$  oven overnight before the weight measurements. After measuring the weight, each specimen was placed back to the incubator in 10 mL of fresh saline.

Fig. 7 shows Zn/Fe bilayer conductor specimens before the degradation test and after immersion in saline for 24 hours before washing and drying. A significant quantity of residue was observed on the surface of the specimen during degradation in saline. Some of the residue was loosely attached to specimen and can be removed by rinsing the specimens in deionized water.

A pictorial history of the Zn/Fe bilayer conductors over the 300-hour experiment duration is shown in figure 8. Initially, a white oxidation product was observed, consistent with Zn oxidation [35]. As the degradation of the Zn/Fe bi-layer conductors continued, the specimen lost physical integrity, beginning with the thinner coil lines and proceeding to the capacitor plates. As degradation progressed, brown/red iron oxides began to be observed, consistent with the iron oxidation [36], and these oxides were not soluble during rinse.

Four Zn/Fe bilayer specimens of similar nominal initial weight (within 7%) were selected for detailed analysis. The normalized average weight loss as a function of degradation time is plotted in Fig. 9. Four specimens show similar degradation behavior: the weight of the specimens monotonically decreased over 200 hours, reaching an asymptotic residual weight of approximately 20% of the original weight.

To further understand the detail of this degradation behavior, the average rate of weight loss as a function of degradation time of the Zn/Fe bilayer is plotted in Fig. 10. The degradation rate can be roughly divided into 3 stages. In the

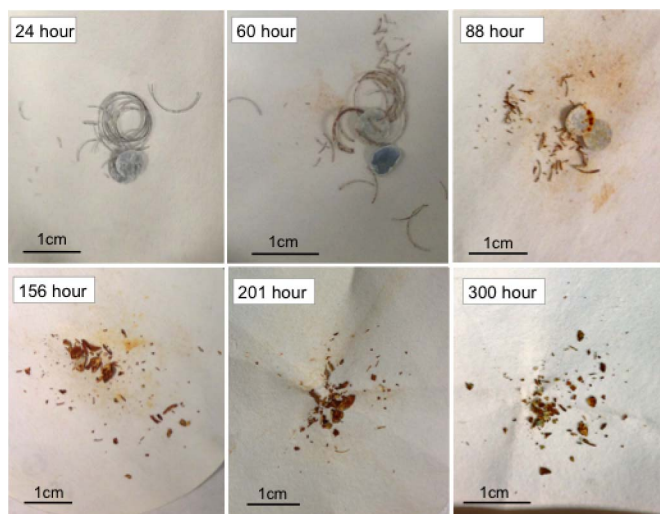


Fig. 8. A pictorial history of the Zn/Fe bilayers conductors over the 300-hour experiment duration.

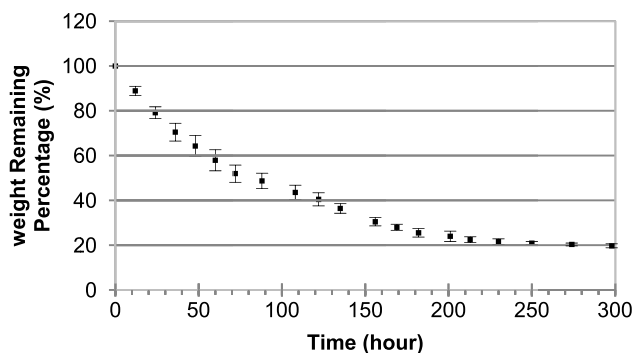


Fig. 9. Remaining weight in percentage of the Zn/Fe bilayer conductor specimens for degradation measurement *in vitro*.

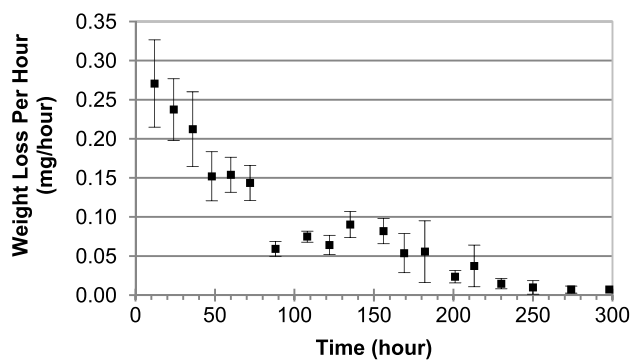


Fig. 10. Weight loss rate (mg/hour) of the Zn/Fe bilayer conductor specimens as function of degradation time in saline.

first 72 hours (stage 1), the degradation rate is the fastest, above 0.15 mg/hour. This stage corresponds to the period that specimens were either unbroken or broken into relatively large pieces, in which the degradation of the Zn/Fe bilayer structure was consistent with a galvanic corrosion mechanism. In stage 2, between 84 and 180 hours, the degradation rate of the bi-layer specimen is between 0.05-0.1 mg/hour. In this stage, the specimens had broken into much smaller pieces,

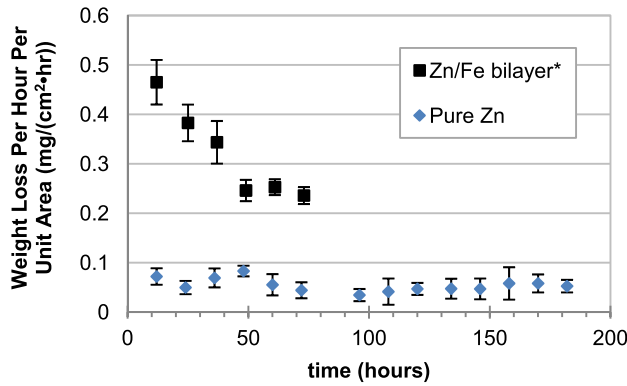


Fig. 11. The weight loss rate per unit area of exposed Zn ( $\text{mg}/(\text{cm}^2 \cdot \text{hr})$ ) of the Zn/Fe bilayer conductor specimens and pure Zn rectangular specimens *in vitro*.

some of which may no longer have been bearing Zn, and initial formation of iron oxides was observed. This slower iron oxidation, together with the reduced Zn surface area as degradation proceeds, is consistent with the observed reduction in weight loss rate. In stage 3, after 200 hours, the degradation rate of the specimens is very small ( $<0.04 \text{ mg}/\text{hour}$ ). In this period, the entire specimen had been broken into very small pieces (Fig. 8). Most of the zinc was gone, leaving only the iron oxide. The total weight of the corroded specimens at the end of stage 3 was approximately 20% of the original weight (Fig. 9), which corresponds to the expected weight of remaining iron if it had been transformed into iron oxides. The residue of the corroded iron cannot be dissolved in saline; however, *in-vivo* studies of iron implants that have undergone biodegradation have shown both lack of toxicity of any residual iron oxides [12, 37] as well as postulated phagocytic transport of iron oxide particles away from the implant site [38].

It is useful to assess the effect of the increase in degradation rate due to galvanic corrosion by comparing the weight loss rates of Zn/Fe bilayers with that of electroplated Zn control specimens (described above). Zn-only rectangular samples did suffer reduction in weight but did not lose physical integrity during the duration of the degradation test (approximately 220 hours).

Since the Zn and Zn/Fe bilayer samples differed in shape, an appropriate way to compare these results is to normalize the weight loss rate for each by the exposed Zn area. Fig. 12 shows the weight loss rate per unit area of exposed Zn for both the Zn ( $A_{\text{Zn}} = 1.50 \text{ cm}^2$ ) and Zn/Fe bilayer ( $A_{\text{bilayer}} = 0.62 \text{ cm}^2$ ) samples. The Zn-only samples exhibited a relatively constant weight loss rate per unit area of exposed Zn of  $0.07 \text{ mg}/(\text{cm}^2 \cdot \text{hr})$ . Since the bilayer samples only had a well-defined exposed Zn area during stage 1 of their degradation, only this stage was plotted in Fig. 11 for comparison. As expected, the degradation rate of the Zn/Fe bilayer structure exceeds that of Zn alone, demonstrating the accelerating effect of galvanic corrosion. The weight loss rate of the Zn/Fe bilayer structure was ten fold higher than that of pure Zn,  $0.46 \text{ mg}/(\text{cm}^2 \cdot \text{hr})$  versus  $0.07 \text{ mg}/(\text{cm}^2 \cdot \text{hr})$  (Fig. 11). This significant change in weight loss rate illustrates the ability to

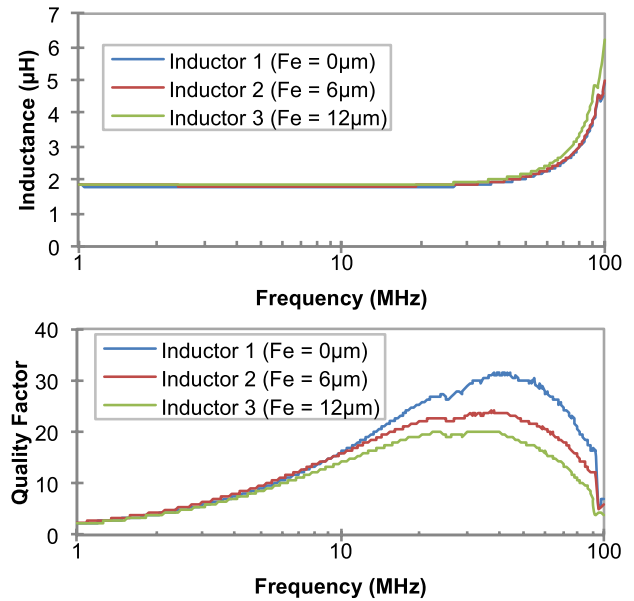


Fig. 12. Inductance (top), and quality factor (bottom) of the Zn/Fe bilayer inductors with different Fe thickness (inductors #2 and #3) and Zn-only inductor (inductor #1). Total metal thickness (Zn + Fe) was held to a nominal 65 micron total.

tailor the degradation rate of the Zn through modulation of the Zn to Fe exposed surface area ratio. Considerations that may affect the designed Zn degradation lifetime include the desire to set the functional lifetime of the sensor as well as limiting the degradation rate to one well-tolerated *in-vivo*.

### B. Inductance and Quality Factor of Inductor

Prior to folding and laminating the embossing film bearing the Zn/Fe bilayer inductor and capacitor plates, the inductance and quality factor of the inductor pattern was measured using an impedance analyzer. Referring to Fig. 6(b), the impedance analyzer probes were placed on the two capacitor plates. The measured inductance and quality factor of the inductor as a function of frequency and parameterized by Fe thickness is shown in Fig. 12. The total metal thickness (Zn + Fe) of the inductors was held constant at approximately  $65 \mu\text{m}$ . An inductance of approximately  $1.9 \mu\text{H}$  was observed at frequencies below 50 MHz independent of the relative thicknesses of Zn and Fe. At higher frequencies, the quality factor ( $Q$ ) decreases as the relative thickness of Fe increases, due to the known poor AC conductance of Fe at higher frequencies.

### C. Wireless Pressure Sensor Characterization

The fabricated pressure sensor was characterized using wireless measurements by inductive coupling with an external coil. The external coil (5 turns, diameter = 1 cm) had no self-resonances in the measurement frequency range. The coil was held at a distance of approximately 3 mm from the sensor. The phase and magnitude of the coil impedance was then measured as a function of frequency using an impedance analyzer [16]. The observation that no resonant frequency shift took place when the distance between the sensor and the coil

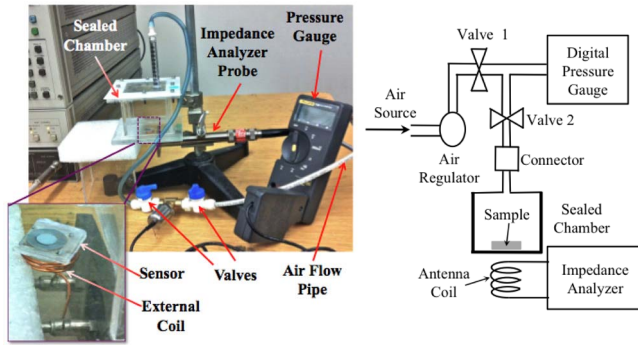


Fig. 13. Pressure sensor test measurement setup (left) with schematic drawing (right).

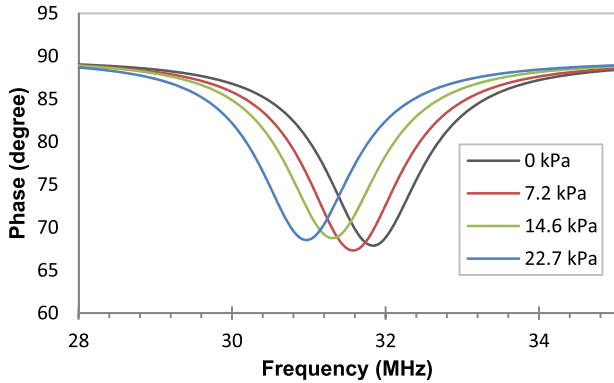


Fig. 14. Measured impedance phase as a function of frequency for several applied pressures.

was changed suggests that the sensor and the external coil are weakly coupled. In the weakly coupled case, there is negligible difference between the measured frequency of phase minimum and the resonant frequency of the sensor [16].

To determine the pressure sensitivity of the fabricated sensor, the sensor is placed in a sealed chamber instrumented with a pressure gauge (Fig. 13). The internal pressure of the chamber was controlled by application of compressed air via an external source. The chamber pressure is controlled by means of a regulator over pressures ranging from 0 to 20 kPa. The electrical response of the sensor was measured at multiple discrete pressure values over this range.

The sensor was first measured using an air environment within the chamber. The measured phase of the external coil as a function of frequency for several applied pressure values is shown in Fig. 14. As the applied pressure is increased, the frequency at which the phase minimum occurs shifts monotonically to lower frequencies. This frequency is very close to the sensor resonant frequency under these measurement conditions [2]. The frequency shift is due to the pressure-induced deflection of the PLLA/metal sensor plates, resulting in a decrease in the capacitor gap, and therefore an increase in capacitance and decrease in resonant frequency. The pressure scan was then repeated to assess the reproducibility of the impedance measurement.

After pressure measurement in air was completed, pressure measurement in saline at room temperature was performed.

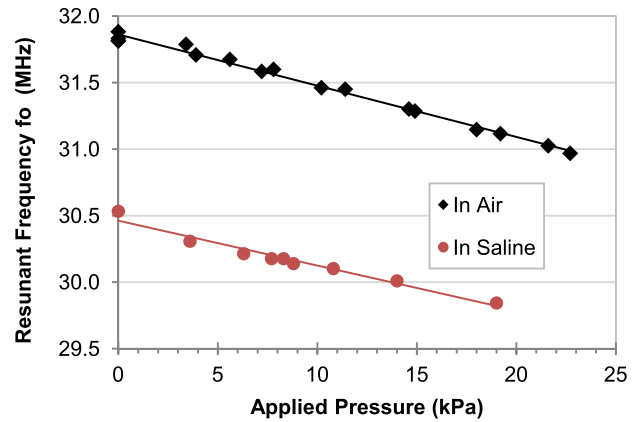


Fig. 15. Resonant frequency ( $f_0$ ) of the pressure sensor as a function of applied pressure in the sealed chamber in air and 0.9% saline environments (within 30-minute immerse time).

The chamber was filled with a saline solution (0.9% NaCl in DI water) to a depth of approximately 5 mm. The sensor was then immersed in saline and the pressure-response measurement was done after the chamber was sealed. Following this test, to investigate the stability and functional lifetime of the sensor, a long-term immersion test was performed. The test consisted of holding the sensor immersed in saline at zero applied pressure for approximately 200 hours. Intermittently during this test, and while immersed in saline, pressure-response measurements were taken to assess sensor sensitivity. These measurements occurred at immersion time points 0-hour, 8-hour, 26-hour, 34-hour, 57-hour, 79-hour and 96-hours.

Fig. 15 shows the resonant frequency of the sensor in air and in saline (within 30-minute immerse time) as a function of applied pressure. In air, the sensor had a resonant frequency of 31.9 MHz at zero applied pressure. From the measured resonant frequency of the sensor and the inductance of the Zn/Fe bilayer inductor before folding to form the device, the calculated capacitance of the sensor without applying pressure in the air environment is 13.8 pF, which is 4.4 pF higher than the analytical calculated result with the initial gap between the capacitor plates set 30  $\mu\text{m}$  (the thickness of the PLLA spacer). The relatively higher value of capacitance of the sensor is consistent with the observation that the bilayer capacitor plates were slightly bent inward after fabrication, due perhaps to thermal effects and/or nonideal lamination. As the applied pressure was increased, the resonant frequency decreased as expected. A sensitivity of  $-39$  MHz/kPa was obtained, which corresponded to  $\Delta C/C_0 = 5.0\%$  over the pressure range 0-20 kPa. Upon immersion of the sensor in saline, the sensor resonant frequency fell from 31.9 MHz to 30.5 MHz and the Q decreased from 20.8 to 18.9. A slightly reduced sensitivity ( $-35$  kHz/kPa) of the sensor was also observed. This behavior is consistent with previous non-biodegradable devices [2] and is due to electrical interactions of the sensor with the embedding medium.

The resonant frequency  $f$ , and quality factor  $Q$  of the sensor as a function of immersion time in saline are shown

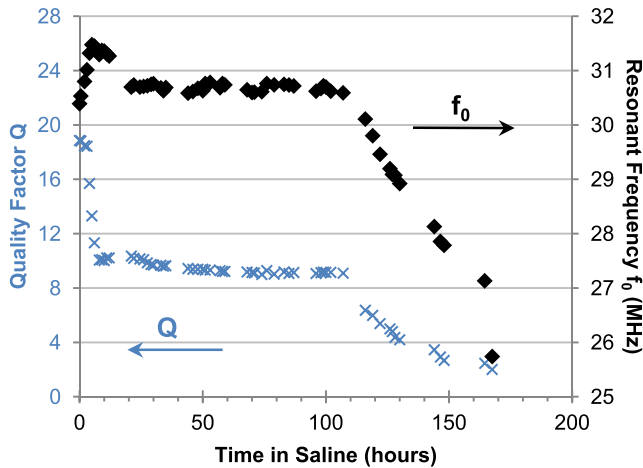


Fig. 16. Calculated quality factor ( $Q$ ) and measured resonant frequency ( $f_0$ ) as a function of the immersion time of the sensor in 0.9% saline without applying pressure.

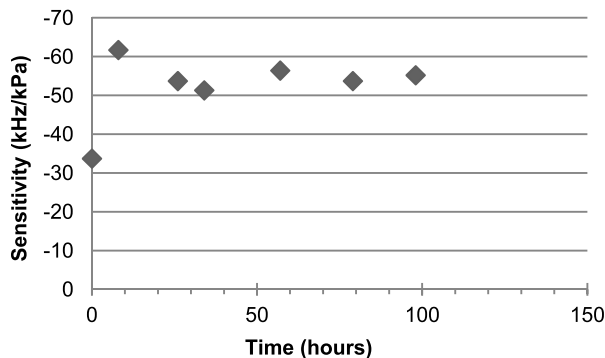


Fig. 17. Measured sensitivity of the pressure sensor after the sensor has been immersed in the saline for 0 hour, 8 hours, 26 hours, 34 hours, 57 hours, 79 hours and 96 hours.

in Fig 16. The performance of the sensor can be divided into three stages. In stage one, within the first 21 hours of immersion, the sensor is observed to equilibrate with the immersion environment. The resonant frequency  $f$  increases rapidly from 30.5 MHz to 31.5 MHz within the first 6 hours and drops gradually to 30.7 MHz, while the  $Q$  drops rapidly from 18.9 to approximately 10 within this time period

In stage two, between 21 to 107 hours, the resonant frequency  $f$  of the sensor remained relatively constant at  $30.7 \pm 0.1$  MHz and the quality factor remained relatively stable above 9.0. Figure 17 shows the sensitivity data acquired during the immersion test. During stage two, the sensitivity also remains relatively stable at  $-54 \pm 4$  kHz/kPa. This sensitivity is slightly higher than that of air, and is consistent with the observation of a small reduction of the Young's modulus of PLLA after immersion in saline [39-41]. As both resonant frequency and sensitivity are relatively stable during stage two, this stage can be considered the functional lifetime during which the sensor can be utilized.

After the sensor had been immersed in saline for 107 hours, the resonant frequency as well as quality factor of the sensor started to drop rapidly (stage three). Very weak resonance between the sensor and the external coil was observed after

168 hours, making it difficult to determine the resonant frequency. The quality factor of the sensor was determined to be smaller than 2. Upon examination, cracks were found in most of the pressure sensors after passing through stage 3. Since PLLA shows brittle behavior at room temperatures [42, 43], the formation of cracks is not unexpected as a failure pathway for these devices.

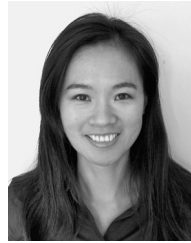
#### IV. CONCLUSION

A RF wireless LC resonant pressure sensor completely made of biodegradable materials was successfully designed, microfabricated and characterized. Microfabrication was achieved by first microfabricating structures on relatively robust substrates and then transferring these structures to biodegradable polymers. The degradation of metallic conductors was shown to be accelerated by a galvanic corrosion mechanism. Fabricated sensors in saline showed three stages of behavior: equilibration, functional lifetime, and performance degradation. In future work, biodegradable polymers with different degradation rates and mechanisms will be studied. Microfabricated biodegradable sensors are expected to have impact in acute or transient biomedical applications as well as use in nonmedical applications where transience and minimal environmental impact are required.

#### REFERENCES

- [1] R. S. Mackay and B. Jacobson, "Endoradiosonde," *Nature*, vol. 197, pp. 1239-1240, Jun. 1957.
- [2] M. A. Fonseca, J. Kroh, J. White, and M. G. Allen, "Flexible wireless passive pressure sensors for biomedical applications," in *Tech. Dig. Solid-State Sens., Actuat., Microsyst. Workshop*, Hilton Head Island, SC, USA, 2006, pp. 37-42.
- [3] M. G. Allen, "Micromachined endovascularly-implantable wireless pressure sensors: From concept to clinic," in *Proc. 13th Int. Conf. Solid-State Sensors, Actuat. Microsyst.*, 2005, pp. 275-278.
- [4] M. Vert, "Bioresorbable polymers for temporary therapeutic applications," *Angew. Makromol. Chem.*, vol. 166, no. 1, pp. 155-168, Feb. 1989.
- [5] X. Zhang, U. P. Wyss, D. Pichora, and M. F. A. Goosen, "An investigation of poly(lactic acid) degradation," *J. Bioactive Compatible Polymers*, vol. 9, no. 1, pp. 80-100, Jan. 1994.
- [6] S. Li and M. Vert, "Biodegradation of aliphatic polyesters," in *Degradable Polymers: Principles and Applications*, G. Scott and D. Gilead, Eds. London, U.K.: Springer-Verlag, 1995, pp. 43-87.
- [7] R. W. Lenz, "Biodegradable polymers," in *Biopolymers I* (Advances in Polymer Science), vol. 107. New York, NY, USA: Springer-Verlag, 1993, pp. 1-40.
- [8] U. Edlund and A.-C. Albertsson, "Degradable polymer microspheres for controlled drug delivery," in *Degradable Aliphatic Polyesters* (Advances in Polymer Science), vol. 157. New York, NY, USA: Springer-Verlag, 2002, pp. 67-112.
- [9] I. Engelberg and J. Kohn, "Physico-mechanical properties of degradable polymers used in medical applications: A comparative study," *Biomaterials*, vol. 12, pp. 292-304, Apr. 1991.
- [10] R. Waksman, "Biodegradable stents: They do their job and disappear," *J. Invasive Cardiol.*, vol. 18, pp. 70-74, Feb. 2006.
- [11] M. P. Staiger, A. M. Pietak, J. Huadmai, and G. Dias, "Magnesium and its alloys as orthopedic biomaterials: A review," *Biomaterials*, vol. 27, pp. 1728-1734, Mar. 2006.
- [12] M. Peuster, P. Wohlsein, M. Brugmann, M. Ehlerding, K. Seidle, C. Fink, *et al.*, "A novel approach to temporary stenting: Degradable cardiovascular stents produced from corrodible metal-results 6-18 months after implantation into new zealand white rabbits," *Heart*, vol. 86, pp. 563-569, Nov. 2001.
- [13] B. Finamore, G. Fedder, A. Khairi, J. Paramesh, L. Schultz, J. Burgess, *et al.*, "Development of an implantable biodegradable electrical stimulator for bone repair," in *Proc. Biomed. Eng. Soc. Fall Meeting*, 2009.

- [14] C. M. Boutry, H. Chandralim, P. Streit, M. Schinhammer, A. C. Hänzi, and C. Hierold, "Characterization of miniaturized RLC resonators made of biodegradable materials for wireless implant applications," *Sens. Actuators A, Phys.*, vol. 189, pp. 344–355, Jan. 2013.
- [15] S. W. Hwang, H. Tao, D. H. Kim, H. Cheng, J.-K. Song, E. Rill, *et al.*, "A physically transient form of silicon electronics," *Science*, vol. 337, pp. 1640–1644, Sep. 2012.
- [16] M. A. Fonseca, J. M. English, M. von Arx, and M. G. Allen, "Wireless micromachined ceramic pressure sensor for high-temperature applications," *J. Microelectromech. Syst.*, vol. 11, pp. 337–343, Aug. 2002.
- [17] M. F. Ashby, R. W. Messler, R. Ashana, E. P. Furlani, R. E. Smallman, A. H. W. Ngan, *et al.*, *Engineering Materials and Processes Desk Reference*, Burlington, MA, USA: Elsevier, 2009, pp. 121–156.
- [18] O. I. Velikokhatnyi and P. N. Kumta, "First-principles studies on alloying and simplified thermodynamic aqueous chemical stability of calcium-, zinc-, aluminum-, yttrium- and iron-doped magnesium alloy," *Acta Biomater.*, vol. 6, pp. 1698–1704, May 2010.
- [19] G. Song, "Control of biodegradation of biocompatible magnesium alloys," *Corros. Sci.*, vol. 49, no. 4, pp. 1696–1701, 2007.
- [20] S. Zhang, X. Zhang, C. Zhao, J. Li, Y. Song, C. Xie, *et al.*, "Research on an Mg-Zn alloy as a degradable biomaterial," *Acta Biomater.*, vol. 6, pp. 626–640, Feb. 2010.
- [21] B. Zberg, P. J. Uggowitzner, and J. F. Löffler, "MgZnCa glasses without clinically observable hydrogen evolution for biodegradable implants," *Nature Mater.*, vol. 8, pp. 887–891, Nov. 2009.
- [22] Y. B. Wang, X. H. Xie, H. F. Li, X. L. Wang, M. Z. Zhao, E. W. Zhang, *et al.*, "Biodegradable CaMgZn bulk metallic glass for potential skeletal application," *Acta Biomater.*, vol. 7, pp. 3196–3208, Aug. 2011.
- [23] P. K. Bowen, J. Drelich, and J. Goldman, "Zinc exhibits ideal physiological corrosion behavior for bioabsorbable stents," *Adv. Mater.*, vol. 25, pp. 2577–2582, May 2013.
- [24] M. Luo, C. Song, F. Herrault, and M. G. Allen, "A microfabricated RF wireless pressure sensor made completely of biodegradable materials," in *Proc. 14th Solid-State Sensors, Actuator, Microsyst. Workshop*, Hilton Head Island, SC, USA, 2012, pp. 38–41.
- [25] F. C. Porter, *Zinc Handbook: Properties, Processing, and use in Design*. New York, NY, USA: Marcel Dekker, 1991, pp. 128–141.
- [26] R. Windand, "Electrodeposition of zinc and zinc alloys," in *Modern Electroplating*, 4th ed., M. Schlesinger and M. Paunovic, Eds. Hoboken, NJ, USA: Wiley, 2010, pp. 423–460.
- [27] M. Izaki, "Electrodeposition of iron and iron alloys," in *Modern Electroplating*, 4th ed., M. Schlesinger and M. Paunovic, Eds. Hoboken, NJ, USA: Wiley, 2010, pp. 461–482.
- [28] T. Kawamoto and T. Sugahara, "Examination of properties of bioabsorbable osteosynthetic material using finite element method," *J. Hard Tissue Biol.*, vol. 14, no. 2, pp. 65–66, 2005.
- [29] H. M. Ledbetter, "Elastic properties of zinc: A compilation and a review," *J. Phys. Chem. Ref. Data*, vol. 6, no. 4, pp. 1181–1203, 1977.
- [30] T. Nakagawa, T. Nakiri, R. Hodoya, and Y. Tajitsu, "Electrical properties of biodegradable polylactic acid film," *IEEE Trans. Ind. Appl.*, vol. 40, no. 4, pp. 1020–1024, Jul. 2004.
- [31] W. Schäfer, P. Abrams, L. Liao, A. Mattiasson, F. Pesce, A. Spangberg, *et al.*, "Good urodynamic practices: Uroflowmetry, filling cystometry, and pressure-flow studies," *Neurourol. Urodynam.*, vol. 21, pp. 261–274, Mar. 2002.
- [32] P. L. Reilly and R. Bullock, *Head Injury: Pathophysiology and Management of Severe Closed Injury*. London, U.K.: Chapman & Hall, 1997.
- [33] C. M. Boutry, R. Kiran, F. Umbrecht, and C. Hierold, "Processing and quantitative analysis of biodegradable polymers (PLLA and PCL) thermal bonding," *J. Micromech. Microeng.*, vol. 20, pp. 1–13, Aug. 2010.
- [34] F. Herrault, S. Yorish, T. M. Crittenden, C.-H. Ji, and M. G. Allen, "Parylene-insulated ultradense microfabricated coils," *J. Microelectromech. Syst.*, vol. 19, pp. 1277–1283, Dec. 2010.
- [35] I. S. Cole, T. H. Muster, D. Lau, N. Wright, and N. S. Azmat, "Products formed during the interaction of seawater droplets with zinc surfaces," *J. Electrochem. Soc.*, vol. 157, pp. C213–C222, Apr. 2010.
- [36] M. Moravej, A. Purnama, M. Fiset, J. Couet, and D. Mantovani, "Electroformed pure iron as a new biomaterial for degradable stents: *In vitro* degradation and preliminary cell viability studies," *Acta Biomater.*, vol. 6, pp. 1843–1851, May 2010.
- [37] M. Peuster, C. Hesse, T. Schloo, C. Fink, P. Beerbaum, and C. von Schnakenburg, "Long-term biocompatibility of a corrodible peripheral iron stent in the porcine descending aorta," *Biomaterials*, vol. 27, pp. 4955–4962, Oct. 2006.
- [38] P. P. Mueller, S. Arnold, M. Badar, D. Bormann, F.-W. Bach, A. Drynda, *et al.*, "Histological and molecular evaluation of iron as degradable medical implant material in a murine animal model," *J. Biomed. Mater. Res. A*, vol. 100, pp. 2881–2889, May 2012.
- [39] H. Tsuji and H. Muramatsu, "Blends of aliphatic polyesters. IV. Morphology, swelling behavior, and surface and bulk properties of blends from hydrophobic poly(L-lactide) and hydrophilic poly(vinyl alcohol)," *J. Appl. Polymer Sci.*, vol. 81, pp. 2151–2160, Jun. 2001.
- [40] C. M. Agrawal, K. F. Haas, D. A. Leopold, and H. G. Clark, "Evaluation of poly(L-lactic acid) as a material for intravascular polymeric stents," *Biomaterials*, vol. 13, no. 3, pp. 176–182, 1992.
- [41] D. D. Wright-Charlesworth, D. M. Miller, I. Miskioglu, and J. A. King, "Nanoindentation of injection molded PLA and self-reinforced composite PLA after *in vitro* conditioning for three months," *J. Biomed. Mater. Res. A*, vol. 74, pp. 388–396, Sep. 2005.
- [42] C. Franchini, R. Plesu, J. R. Sarasua, and R. E. Prud'Homme, "Cracking in polylactide spherulites," *J. Polymer Sci. B, Polymer Phys.*, vol. 43, pp. 3308–3315, Oct. 2005.
- [43] L. V. Labrecque, R. A. Kumar, V. Dave, R. A. Gross, and S. P. McCarthy, "Citrate esters as plasticizers for poly(lactic acid)," *J. Appl. Polymer Sci.*, vol. 66, pp. 1507–1513, Dec. 1997.



**Mengdi Luo** received the B.S. degree and M.S. degree in materials science and engineering from Tongji University, Shanghai, China in 2005 and 2008, respectively. She is currently pursuing the Ph.D. degree in materials science and engineering at Georgia Institute of Technology, Atlanta. Her current research interest is mainly in design, microfabrication and characterization of completely biodegradable wireless sensors for implantation applications.



**Adam W. Martinez** received the B.S. degree in biological engineering from Louisiana State University, Baton Rouge, in 2005 and the Ph.D. degree in biomedical engineering from the joint Georgia Institute of Technology and Emory University program, Atlanta in 2011. From 2012 to 2013, he was a Postdoctoral Fellow with the MicroSensors and MicroActuators Group, Georgia Institute of Technology, Atlanta, Georgia. His research was focused on the development of biodegradable materials through synthetic and subtractive strategies, and the utilization of these materials to fabricate biodegradable MEMS based diagnostics, sensors, and power sources. Dr. Martinez's awards and honors include the Technological Innovation: Generating Economic Results Fellowship, NSF Graduate Research Fellowship, Pittsburgh Tissue Engineering Award, and Howard Hughes Undergraduate Research Fellowship.



**Chao Song** received a B.S. degree in electrical engineering from Shanghai Jiaotong University in 2004. In 2007, he obtained his Dipl.-Ing in electronic and signal processing and an M.S. degree in microelectronics circuits and microsystems from ENSEIHT, Toulouse, France. In 2008, he received his M.S. degree in electrical and computer engineering from Georgia Institute of Technology and started working toward his Ph.D. degree in the research group of Professor Mark G. Allen. His current research includes MEMS flow and pressure sensors, implantable pressure sensors, sensor interface circuits, neuron interfacing devices, and power management ICs. From 2004 to 2005, he worked in Chinese Academy of Science Shanghai Institute of Micro-system and Information Technology in the area of sensor network. In 2006, he interned in SIEMENS VDO, Toulouse, France, testing and evaluating a position sensor for automobile. In 2007 he interned in Research Center of Spatial Ray, Toulouse, France, designing interfacing ICs for radiation detection sensors. Since 2008, he has been a research assistant in Georgia Institute of Technology, Atlanta, Georgia. He is currently a design intern in Linear Technology Corporation, Milpitas, California, working on power management ICs.



**Florian Herrault** (M'12) received the B.S. and M.S. degrees in physics and materials science from the National Institute of Applied Sciences (INSA), Toulouse, France, in 2003 and 2005, respectively, and the Ph.D. degree in electrical and electronics engineering from the University of Toulouse in 2009. From 2009 to 2013, he was a Research Engineer with the MicroSensors and MicroActuators Group (Georgia Institute of Technology), and acted as the group's deputy director. His research was focused on integrated magnetics for power supplies on a chip and MEMS based biomedical implants. He is currently a Member of the Technical Staff at HRL Laboratories, developing advanced microfabrication-based packaging technologies for mm-wave components. Dr. Herrault has been a member of the technical program committee and a session co-chair for the International Workshop on Power Supply on Chip 2010 and 2012, and the International Workshop on Micro and Nanotechnology for Power Generation and Energy Conversion Applications (PowerMEMS) 2012 and 2013.



**Mark G. Allen** (M'88–SM'04–F'11) received the B.A. degree in chemistry, the B.S.E. degree in chemical engineering, and the B.S.E. degree in electrical engineering from the University of Pennsylvania, Philadelphia, and the S.M. and Ph.D. (1989) degrees from Massachusetts Institute of Technology, Cambridge. In 1989 he joined the faculty of the School of Electrical and Computer Engineering, Georgia Institute of Technology, Atlanta, ultimately holding the rank of Regents' Professor and the J.M. Pettit Professorship in Microelectronics, as well as a joint appointment in the School of Chemical and Biomolecular Engineering. In 2013 he left Georgia Tech to become the Alfred Fitler Moore Professor of Electrical and Systems Engineering and Scientific Director of the Singh Nanotechnology Center at the University of Pennsylvania in Philadelphia, PA. His research interests are in the development and the application of new micro- and nanofabrication technologies, as well as MEMS. Dr. Allen is the Editor-in-Chief of the *Journal of Micromechanics and Microengineering*, and was a previous co-chair of the IEEE/ASME MEMS Conference.